IEEE Photonics Journal
An IEEE Photonics Society Publication

Open Access

W-Band Millimeter-Wave Vector Signal Generation Based on Precoding-Assisted Random Photonic Frequency Tripling Scheme Enabled by Phase Modulator

Volume 8, Number 2, April 2016

Xinying Li
Yuming Xu
Jiangnan Xiao
Jianjun Yu

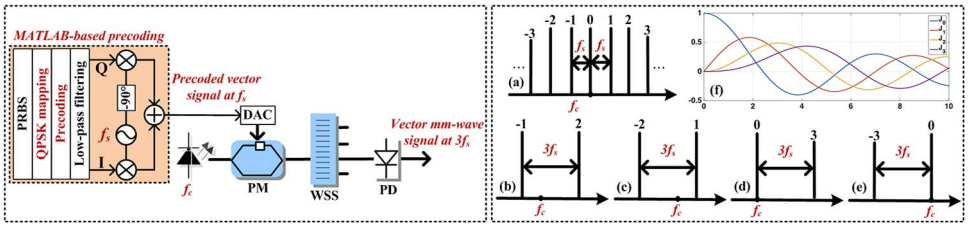

DOI: 10.1109/JPHOT.2016.2535203
1943-0655 © 2016 IEEE

IEEE photonics SOCIETY

IEEE

W-Band Millimeter-Wave Vector Signal Generation Based on Precoding-Assisted Random Photonic Frequency Tripling Scheme Enabled by Phase Modulator

Xinying Li,[1,2,3] Yuming Xu,[1,2,3] Jiangnan Xiao,[1] and Jianjun Yu[1]

[1]Key Laboratory for Information Science of Electromagnetic Waves (MoE), Fudan University, Shanghai 200433, China
[2]Georgia Institute of Technology, Atlanta, GA 30332 USA
[3]ZTE (TX) Inc., Morristown, NJ 07960 USA

DOI: 10.1109/JPHOT.2016.2535203

Manuscript received January 30, 2016; revised February 18, 2016; accepted February 21, 2016. Date of publication February 26, 2016; date of current version March 9, 2016. This work was supported in part by the National "863" Program of China under Grant 2015AA016904 and in part by the National Natural Science Foundation of China under Grant 61325002 and Grant 61527801. Corresponding author: X. Li (e-mail: xinying.li@ece.gatech.edu).

Abstract: We propose W-band photonic millimeter-wave (mm-wave) vector signal generation employing a precoding-assisted random frequency tripling scheme enabled by a single phase modulator cascaded with a wavelength selective switch (WSS). The selected two optical subcarriers from the phase modulator output by the WSS can have several different kinds of combinations with asymmetrical orders, such as (−3, 0), (−2, 1), (−1, 2), and (0, 3). Employing our proposed precoding-assisted random frequency tripling scheme, we experimentally demonstrate 1/2-Gbd 81-GHz quadrature-phase-shift-keying (QPSK) mm-wave vector signal generation and its wireless delivery over 0.5-m air space distance. We also experimentally demonstrate that the generated mm-wave vector signal based on the minus second-order (−2nd) and first-order (1st) subcarriers, which is equivalent to that based on the minus first-order (−1st) and second-order (2nd) subcarriers, has a better bit-error-ratio (BER) performance than that based on the minus third-order (−3rd) and central (0th) subcarriers, which is equivalent to that based on the 0th and third-order (−3rd) subcarriers, when the phase modulator has a relatively small driving radio-frequency (RF) voltage, whereas an opposite result occurs when the phase modulator has a relatively large driving RF voltage, which is consistent with both our theoretical analysis and numerical simulation.

Index Terms: Photonic millimeter-wave (mm-wave) vector signal generation, W-band, random frequency tripling, precoding, quadrature phase shift keying (QPSK).

1. Introduction

Recently, there has been ever-increasing research interest in the application of W-band (75 GHz–110 GHz) with large available bandwidth and vector signal modulation with high spectral efficiency into radio-over-fiber (RoF) systems [1]–[24] in order to meet the demands of emerging large-capacity mobile data communication. Precoding-assisted photonic frequency multiplication techniques based on the electro-optic intensity modulator or the phase modulator [18]–[30] can

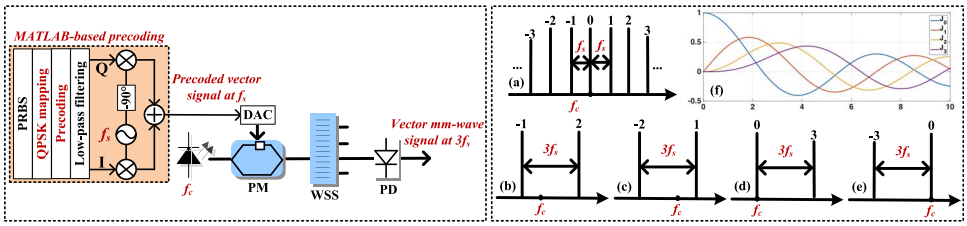

Fig. 1. Schematic diagram of photonic mm-wave vector signal generation based on a precoding-assisted random frequency tripling scheme. (a) Schematic output optical spectrum of phase modulator. (b)–(e) Schematic output optical spectra of WSS. (f) Curves of the first-kind Bessel function from order 0 to order 3. DAC: digital-to-analog converter; PM: phase modulator; WSS: wavelength selective switch; PD: photodiode.

realize simple and cost-effective W-band photonic millimeter-wave (mm-wave) vector signal generation, with the advantages of high stability, high purity, and significantly reduced requirement for transmitter component bandwidth [25]–[35]. Recently, lots of experimental demonstrations on W-band photonic mm-wave vector signal generation have been reported, employing precoding-assisted photonic frequency multiplication techniques based on a single electro-optic intensity modulator or phase modulator [18]–[24]. However, all the previous experimental demonstrations [18]–[24] select from the output of the intensity modulator or phase modulator two optical subcarriers with symmetrical orders to realize photonic frequency multiplication with an even multiplication factor.

In this paper, we propose precoding-assisted random-frequency-tripling W-band photonic mm-wave vector signal generation enabled by a single phase modulator cascaded with a wavelength selective switch (WSS). The selected two optical subcarriers from the phase modulator output by the WSS can have several different kinds of combinations with asymmetrical orders, such as (–3, 0), (–2, 1), (–1, 2), and (0, 3). Employing our proposed precoding-assisted random frequency tripling scheme, we experimentally demonstrate 1/2-Gbaud 81-GHz quadrature-phase-shift-keying (QPSK) mm-wave vector signal generation and its wireless delivery over 0.5-m air space distance. We also experimentally demonstrate that the generated mm-wave vector signal based on the minus second-order (–2nd) and first-order (1st) subcarriers, which are equivalent to those based on the minus first-order (–1st) and second-order (2nd) subcarriers, has a better bit-error-ratio (BER) performance than that based on the minus third-order (–3rd) and central (0th) subcarriers, which is equivalent to that based on the 0th and third-order (3rd) subcarriers, when the phase modulator has a relatively small driving radio-frequency (RF) voltage, while an opposite result occurs when the phase modulator has a relatively large driving RF voltage, which is consistent with both our theoretical analysis and numerical simulation.

2. Principle and Numerical Simulation

2.1. Principle

Fig. 1 shows the schematic diagram of photonic mm-wave vector signal generation, based on a precoding-assisted random frequency tripling scheme, enabled by a single phase modulator cascaded with a WSS. With the aid of MATLAB programming, a pseudo-random binary sequence (PRBS) with a certain length is first QPSK mapped, then precoded and low-pass filtered, and finally digitally up-converted from baseband to frequency f_s, to generate the precoded RF vector signal at frequency f_s [18]. Here, the function of low-pass filtering is implemented by a fifth-order Bessel filter with a cutoff frequency of $2 \times \pi \times B$ (B denotes the signal baud rate).

After processed by a high-speed digital-to-analog converter (DAC), the generated precoded RF vector signal at frequency f_s is modulated by a single phase modulator onto a

continuous-wave (CW) lightwave at frequency f_c from a laser. Assume that the CW lightwave at frequency f_c has constant amplitude E_0 and can be formulated as

$$E_{CW}(t) = E_0 \exp[j2\pi f_c t + j\varphi(t)] \tag{1}$$

where φ denotes the random phase noise induced by laser linewidth. Assume that the driving RF vector signal at frequency f_s has constant amplitude V_0 and can be formulated as

$$V_{\mathrm{RF}}(t) = V_{\mathrm{RF}} V_0 \cos[2\pi f_s t + \theta(t)] \tag{2}$$

where V_{RF} denotes the driving RF voltage on the phase modulator, and θ denotes the precoded phase of the driving RF vector signal at frequency f_s. The phase modulator output can thus be formulated as [24]

$$\begin{aligned} E_{\mathrm{PM}}(t) &= E_0 \exp[j2\pi f_c t + j\varphi(t) + j\pi V_{\mathrm{RF}}(t)/V_\pi] \\ &= E_0 \sum_{n=-\infty}^{\infty} j^n J_n(\kappa) \exp[j2\pi(f_c + nf_s)t + jn\theta(t) + j\varphi(t)] \end{aligned} \tag{3}$$

where J_n is the first-kind Bessel function of order n. κ is equal to $\pi V_{\mathrm{RF}} V_0 / V_\pi$ (V_π denotes the half-wave voltage of the phase modulator), representing the modulation index of the phase modulator. The phase modulator output thus should be multiple optical subcarriers with a frequency spacing of f_s, and Fig. 1(a) gives the schematic output optical spectrum of the phase modulator.

Then, a WSS randomly selects from the phase modulator output two optical subcarriers with a frequency spacing of $3f_s$. The selected two optical subcarriers with a frequency spacing of $3f_s$ can be the −1st one and the 2nd one shown in Fig. 1(b), the −2nd one and the 1st one shown in Fig. 1(c), the 0th one and the 3rd one shown in Fig. 1(d), or the −3rd one and the 0th one shown in Fig. 1(e). As a result, the WSS output can be formulated as

$$\begin{aligned} E_{\mathrm{WSS}}(t) = {} & E_0 j^m J_m(\kappa) \exp[j2\pi(f_c + mf_s)t + jm\theta(t) + j\varphi(t)] \\ & + E_0 j^{m+3} J_{m+3}(\kappa) \exp\{j2\pi[f_c + (m+3)f_s]t + j(m+3)\theta(t) + j\varphi(t)\} \end{aligned} \tag{4}$$

where m can be randomly assigned as −3, −2, −1, or 0. Next, the output current of the single-ended photodiode (PD), in which the selected two optical subcarriers are heterodyne beat, can be formulated as (the DC component is excluded)

$$i_{\mathrm{PD}}(t) = \frac{1}{2} R J_m(\kappa) J_{m+3}(\kappa) \cos[2\pi \cdot 3f_s t + 3\theta(t)] \tag{5}$$

where R denotes the PD sensitivity. As shown by (5), after square-law PD conversion, frequency-tripling electrical mm-wave signal at frequency $3f_s$ is generated, while the random phase noise φ is eliminated because of the frequency-locking and phase-locking characteristic of the selected two optical subcarriers from the same laser source [36].

As also shown by (5), the phase term 3θ of the PD output current carries the precoded phase θ of the driving RF vector signal at frequency f_s. Thus, the value of θ should be appropriately set to ensure that the phase term 3θ of the PD output current satisfies the rule of regular QPSK modulation, in order to make the generated electrical mm-wave signal at frequency $3f_s$ display regular QPSK modulation [18]. Assume that the phase of regular QPSK symbol is represented by θ_{QPSK}. Thus, θ should satisfy $3\theta = \theta_{\mathrm{QPSK}}$ when imbalanced phase precoding is adopted [18], while it should satisfy $3\theta = \theta_{\mathrm{QPSK}} + 2\,m\pi$ ($m = 0, 1, 2$) when balanced phase precoding is adopted [30]. Moreover, the amplitude of the generated electrical mm-wave signal, which determines the signal-to-noise ratio (SNR) after PD detection, are determined by $J_m(\kappa)J_{m+3}(\kappa)$ as shown by (5). Since $|J_{-2}(\kappa)J_1(\kappa)|$ is equal to $|J_{-1}(\kappa)J_2(\kappa)|$ while $|J_{-3}(\kappa)J_0(\kappa)|$ is equal to $|J_0(\kappa)J_3(\kappa)|$, we can conclude that, the generated mm-wave vector signal based on the −2nd and 1st subcarriers is equivalent to that based on the −1st and 2nd subcarriers, while the generated mm-wave vector signal based on the −3rd and 0th subcarriers is equivalent to that based on the 0th and 3rd subcarriers. Fig. 1(f) shows the curves of the first-kind Bessel

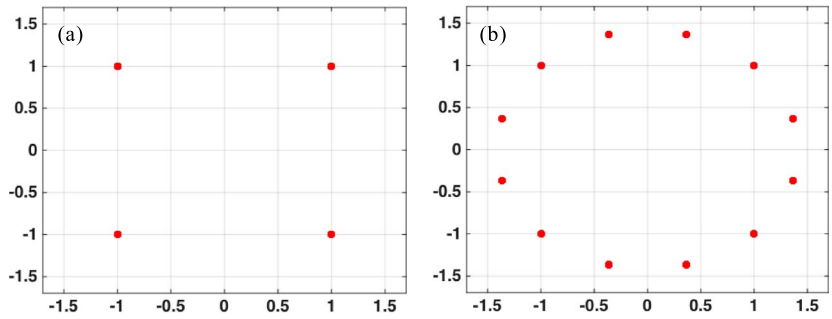

Fig. 2. (a) Calculated constellation after QPSK mapping. (b) Calculated constellation after balanced phase precoding.

function from order 0 to order 3 when the modulation index κ varies from 0 to 10. We can see that, with the increase of the modulation index κ, or the increase of the driving RF voltage V_{RF} on the phase modulator, more and more optical subcarriers appear, and the orders of the optical subcarriers with relatively high optical power also gradually increase. Since the optical power of the selected optical subcarriers determines the SNR after PD detection, we can anticipate that, the generated electrical mm-wave vector signal at frequency $3f_s$ based on the −2nd and 1st (or −1st and 2nd) subcarriers has a better performance than that based on the −3rd and 0th (0th and 3rd) subcarriers when V_{RF} is relatively small, while an opposite result occurs when V_{RF} is relatively large. It is worth noting that the optical subcarriers with orders higher than 3 theoretically can be also selected to realize frequency tripling, but in this case, a much larger driving RF voltage is required to ensure that the optical subcarriers with orders higher than 3 have a sufficient optical power, which, however, is difficult to achieve in the experiment because of the limited electrical amplifier (EA) amplification. Therefore, in the following numerical simulation and experiment, we do not consider the optical subcarriers with orders higher than 3 for random photonic frequency tripling.

2.2. Numerical Simulation

With the aid of VPI software, we numerically investigate the effect of the driving RF voltage V_{RF} of the phase modulator on the performance of the generated QPSK mm-wave vector signal by our proposed precoding-assisted random frequency tripling scheme. The time window is 128 ns and the sampling rate is 512 GSa/s. The phase modulator is driven by a 27-GHz RF vector signal generated by MATLAB programming, adopting balanced phase precoding and carrying 4-Gbaud QPSK vector data. The pattern length is 2^{10}. Fig. 2(a) gives the calculated constellation after QPSK mapping, while Fig. 2(b) gives that after balanced phase precoding. The selected two optical subcarriers used for square-law PD conversion is the −2nd and 1st ones, or the −3rd and 0th ones, to generate the 81-GHz QPSK-modulated electrical mm-wave vector signal. The down conversion of the generated 81-GHz electrical mm-wave vector signal into baseband is also implemented by MATLAB programming.

Fig. 3(a)–(i) give the calculated optical spectra of the phase modulator output, corresponding to 1.0-, 1.2-, 1.4-, 1.6-, 1.8-, 2.0-, 2.2-, 2.4-, and 2.6-V driving RF voltages on the phase modulator, respectively. For the two calculated received QPSK constellations inserted into each optical spectrum in Fig. 3, the left one corresponds to the generated electrical mm-wave vector signal based on the −2nd and 1st subcarriers, while the right one corresponds to that based on the −3rd and 0th subcarriers. We can see that, the left constellation has a better performance than the right one when the driving RF voltage is relatively small, such as Fig. 3(a) and (b), while the right constellation has a better performance than the left one when the driving RF voltage is relatively large, such as Fig. 3(d)–(g), which is consistent with our theoretical analysis in Section 2.1. Both the left and right constellations in Fig. 3(h) and (i) have a relatively poor performance since

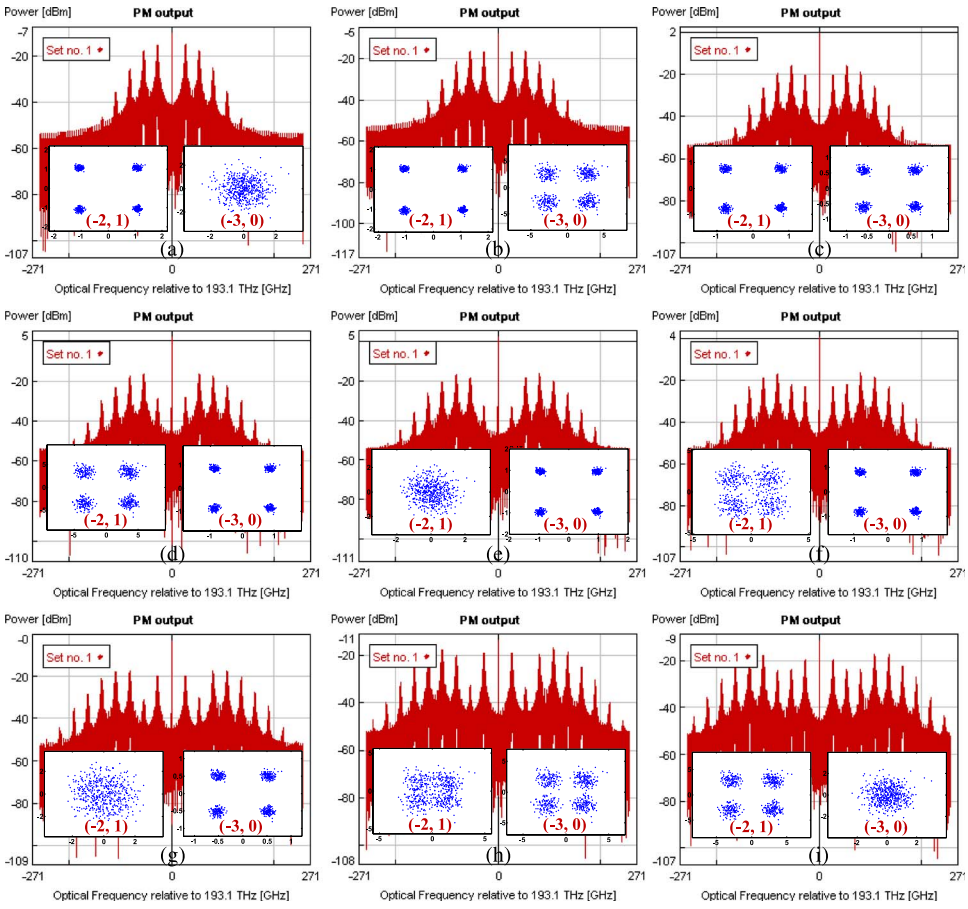

Fig. 3. Calculated optical spectra of phase modulator output and corresponding received constellations when the driving RF voltages on the phase modulator are (a) 1.0 V, (b) 1.2 V, (c) 1.4 V, (d) 1.6 V, (e) 1.8 V, (f) 2.0 V, (g) 2.2 V, (h) 2.4 V, and (i) 2.6 V, respectively.

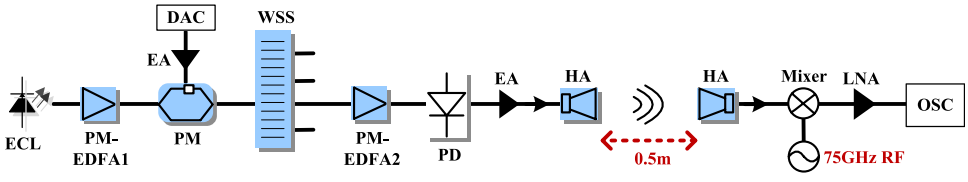

Fig. 4. Experimental setup for the generation and wireless delivery of W-band QPSK mm-wave vector signal employing our proposed precoding-assisted random frequency tripling scheme. ECL: external cavity laser; PM-EDFA: polarization-maintaining Erbium-doped fiber amplifier; PM: phase modulator; DAC: digital-to-analog converter; EA: electrical amplifier; WSS: wavelength selective switch; PD: photodiode; HA: horn antenna; RF: radio frequency; LNA: low-noise amplifier; OSC: oscilloscope.

more optical power is transferred to the optical subcarriers with orders higher than 3 at higher driving RF voltages of 2.4 V and 2.6 V.

3. Experimental Setup

Fig. 4 shows the experimental setup for the generation and wireless delivery of W-band QPSK mm-wave vector signal employing our proposed precoding-assisted random frequency tripling scheme. A 27-GHz balanced-precoded RF vector signal generated by MATLAB programming

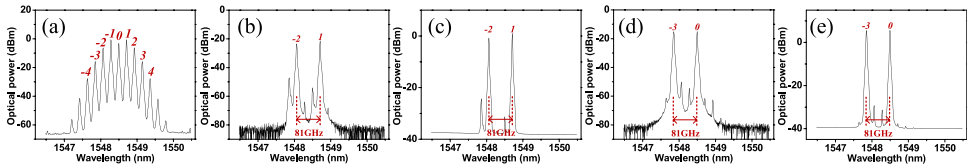

Fig. 5. Measured optical spectra (0.02-nm resolution) when the driving RF voltage on the phase modulator is 4 V_{pp}. (a) After phase modulator, (b) after WSS when the −2nd and 1st subcarriers are selected, (c) after PM-EDFA2 when the −2nd and 1st subcarriers are selected, (d) after WSS when the −3rd and 0th subcarriers are selected, and (e) after PM-EDFA2 when the −3rd and 0th subcarriers are selected.

carries 1- or 2-Gbaud QPSK vector data and has a pattern length of 2^{10}. After processed by a DAC with a sampling rate of 80 GSa/s and a 3-dB electrical bandwidth of 16 GHz, the 27-GHz balanced-precoded RF vector signal is boost to $\sim$4 V_{pp} (or $\sim$9 V_{pp}, which is the maximum driving RF voltage our experimental setup can offer) by an EA operating within the frequency range from 17 GHz to 27 GHz, and then used to drive a phase modulator with 3.5-V half-wave voltage at 1 GHz, 3.5-dB insertion loss, and 40-GHz 3-dB optical bandwidth. A CW lightwave offered by an external cavity laser (ECL) with a linewidth below 100 kHz and an output power of 13 dBm, is first boost by a polarization-maintaining Erbium-doped fiber amplifier (denoted by PM-EDFA1), and then modulated by the 27-GHz balanced-precoded RF vector signal via the phase modulator.

Two subcarriers with 81-GHz frequency spacing are selected from the phase modulator output by a programmable 1 $\times$ 4 WSS on a 10-GHz grid to generate the 81-GHz optical mm-wave signal. The orders of the selected two subcarriers can be a random one of the four cases shown in Fig. 1(b)–(e). The generated 81-GHz optical mm-wave signal is boost by another polarization-maintaining Erbium-doped fiber amplifier (denoted by PM-EDFA2) and then up-converted into an 81-GHz QPSK-modulated electrical mm-wave vector signal by a single-ended W-band PD with 90-GHz optical bandwidth. After boost by a W-band EA with a gain of 30 dB and a saturation output power of 3 dBm, the up-converted 81-GHz QPSK-modulated electrical mm-wave vector signal is delivered over 0.5-m air space distance by a pair of W-band horn antennas (HAs) with a gain of 25 dBi and a 3-dB half-power beamwidth of 10^0.

At the wireless receiver, the received 81-GHz QPSK-modulated electrical mm-wave vector signal is down-converted into a lower frequency 6-GHz one by a balanced mixer, which is driven by a 75-GHz sinusoidal RF source with 16-dBm output power. After boost by a DC~40 GHz low-noise amplifier (LNA) with a gain of 33 dB, the down-converted 6-GHz signal is captured by a real-time digital storage oscilloscope (OSC) with an electrical bandwidth of 30 GHz and a sampling rate of 80 GSa/s. Finally, offline digital signal processing (DSP), including down conversion, constant-modulus-algorithm (CMA) equalization, carrier recovery, and BER calculation [37], is adopted to recover the transmitted QPSK vector data from the 6-GHz signal.

4. Experimental Results

We experimentally investigate the performance of the generated 81-GHz QPSK-modulated mm-wave vector signal when the phase modulator has a relatively small driving RF voltage of 4 V_{pp} and a relatively large driving RF voltage of 9 V_{pp}, respectively.

4.1. Experimental Results When the Phase Modulator has a Relatively Small Driving RF Voltage of 4 V_{pp}

Fig. 5 gives the optical spectra (all measured at 0.02-nm resolution and 1 Gbaud) when the driving RF voltage on the phase modulator is 4 V_{pp}. Fig. 5(a) gives the optical spectrum of the phase modulator output, with multiple optical subcarriers spaced by 27 GHz. Fig. 5(b) and (c), respectively, show the output optical spectra of the WSS and the PM-EDFA2 when the −2nd and 1st

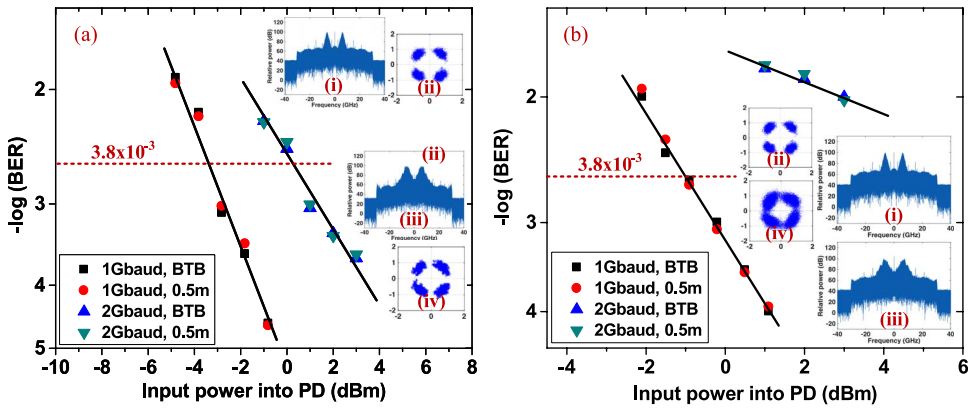

Fig. 6. (a) Measured BER performance at 4-V_{pp} driving RF voltage on the phase modulator. (a) Scenario when the −2nd and 1st subcarriers are selected. (b) Scenario when the −3rd and 0th subcarriers are selected.

subcarriers are selected, while Fig. 5(d) and (e) show those when the −3rd and 0th subcarriers are selected.

We further measured the BER performance versus the input power into PD when the driving RF voltage on the phase modulator is 4 V_{pp}, just as shown in Fig. 6. Fig. 6(a) corresponds to the scenario when the −2nd and 1st subcarriers are selected. It can be seen from Fig. 6(a) that, compared to the 1-Gbaud case, the 2-Gbaud case has a 4-dB power penalty at the BER of 3.8×10^{-3}. 0.5-m wireless delivery causes no power penalty for both 1-Gbaud and 2-Gbaud cases. In Fig. 6(a), insets (i) and (ii) respectively give the captured 6-GHz signal spectrum and the recovered QPSK constellation for the 1-Gbaud mm-wave vector signal after 0.5-m wireless delivery at 1-dBm input power into PD, while insets (iii) and (iv) give those for the 2-Gbaud mm-wave vector signal after 0.5-m wireless delivery at 5-dB input power into PD. Fig. 6(b) corresponds to the scenario when the −3rd and 0th subcarriers are selected. It can be seen from Fig. 6(b) that the 1-Gbaud case can reach the BER of 3.8×10^{-3} when the input power into PD is −1 dBm, while the 2-Gbaud case has an error floor close to the BER of 1×10^{-2}. 0.5-m wireless delivery causes no power penalty for both 1-Gbaud and 2-Gbaud cases. In Fig. 6(b), insets (i) and (ii), respectively, give the captured 6-GHz signal spectrum and the recovered QPSK constellation for the 1-Gbaud mm-wave vector signal after 0.5-m wireless delivery at 3.1-dBm input power into PD, while insets (iii) and (iv) give those for the 2-Gbaud mm-wave vector signal after 0.5-m wireless delivery at 3-dB input power into PD.

When we compare Fig. 6(a) and (b), we can see that, the 1-Gbaud case in Fig. 6(a) has a 2-dB receiver sensitivity improvement compared to that in Fig. 6(b), while the 2-Gbaud case in Fig. 6(a) has a much better BER performance compared to that in Fig. 6(b). We also measured the BER performance in the scenario when the −1st and 2nd subcarriers are selected, which is quite similar to that given in Fig. 6(a), as well as that in the scenario when the 0th and 3rd subcarriers are selected, which is quite similar to that given in Fig. 6(b). Thus, we can conclude that, when the phase modulator has a relatively small driving RF voltage of 4 V_{pp}, the generated 81-GHz QPSK-modulated mm-wave vector signal based on the −2nd and 1st (−1st and 2nd) subcarriers has a better BER performance than that based on the −3rd and 0th (0th and 3rd) subcarriers, which is consistent with both our theoretical analysis and numerical calculation.

4.2. Experimental Results When the Phase Modulator has a Relatively Large Driving RF Voltage of 9 V_{pp}

Fig. 7 gives the optical spectra (all measured at 0.02-nm resolution and 1 Gbaud) when the driving RF voltage on the phase modulator is 9 V_{pp}. Fig. 7(a) gives the optical spectrum of the phase modulator output. Fig. 7(b) and (c) respectively show the output optical spectra of the WSS and the

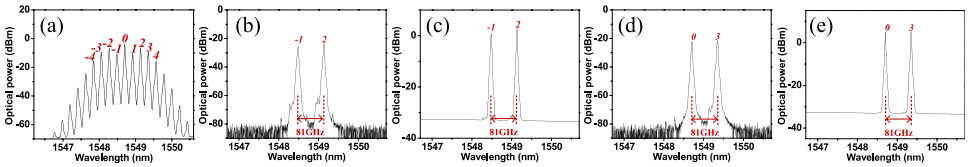

Fig. 7. Measured optical spectra (0.02-nm resolution) when the driving RF voltage on the phase modulator is 9 V_{pp}. (a) After phase modulator, (b) after WSS when the −1st and 2nd subcarriers are selected, (c) After PM-EDFA2 when the −1st and 2nd subcarriers are selected, (d) after WSS when the 0th and 3rd subcarriers are selected, and (e) after PM-EDFA2 when the 0th and 3rd subcarriers are selected.

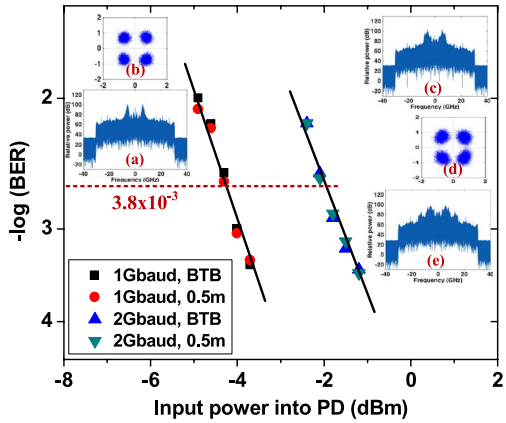

Fig. 8. Measured BER performance at 9-V_{pp} driving RF voltage on the phase modulator in the scenario when the 0th and 3rd subcarriers are selected. Insets (a) and (b), respectively, give the captured 6-GHz signal spectrum and the recovered QPSK constellation for the 1-Gbaud mm-wave vector signal after 0.5-m wireless delivery at −1.1-dBm input power into PD, while insets (c) and (d) give those for the 2-Gbaud mm-wave vector signal after 0.5-m wireless delivery at −0.2-dB input power into PD. Inset (e) gives the captured evidently expanded 6-GHz signal spectrum for the 1-Gbaud mm-wave vector signal after 0.5-m wireless delivery at 0.5-dBm input power into PD in the scenario when the −1st and 2nd subcarriers are selected.

PM-EDFA2 when the −1st and 2nd subcarriers are selected, while Fig. 7(d) and (e) show those when the 0th and 3rd subcarriers are selected.

We further measured the BER performance versus the input power into PD at 9-V_{pp} driving RF voltage on the phase modulator in the scenario when the 0th and 3rd subcarriers are selected, just as shown in Fig. 8. It can be seen from Fig. 8 that, compared to 1-Gbaud case, 2-Gbaud case has a 2.5-dB power penalty at the BER of 3.8×10^{-3}. 0.5-m wireless delivery causes no power penalty for both 1-Gbaud and 2-Gbaud cases. In Fig. 8, insets (a) and (b) respectively give the captured 6-GHz signal spectrum and the recovered QPSK constellation for the 1-Gbaud mm-wave vector signal after 0.5-m wireless delivery at −1.1-dBm input power into PD, while insets (c) and (d) give those for the 2-Gbaud mm-wave vector signal after 0.5-m wireless delivery at −0.2-dB input power into PD. However, when the driving RF voltage on the phase modulator is 9 V_{pp}, we cannot successfully recover the received mm-wave vector signal in the scenario when the −1st and 2nd subcarriers are selected. Inset (e) in Fig. 8 gives the captured 6-GHz signal spectrum for the 1-Gbaud mm-wave vector signal after 0.5-m wireless delivery at 0.5-dBm input power into PD in the scenario when the −1st and 2nd subcarriers are selected, and here we can see that the signal spectrum is evidently expanded. We also measured the BER performance in the scenario when the −3rd and 0th subcarriers are selected, which is quite similar to that given in Fig. 8(a), as well as the BER performance in the scenario when the −2nd and 1st subcarriers are selected, which is quite similar to that in the scenario when the −1st and 2nd subcarriers are selected. Thus, we can conclude that, when the phase

modulator has a relatively large driving RF voltage of 9 V_{pp}, the generated 81-GHz QPSK-modulated mm-wave vector signal based on the 0th and 3rd (–3rd and 0th) subcarriers has a better BER performance than that based on the –1st and 2nd (–2nd and 1st) subcarriers, which is also consistent with both our theoretical analysis and numerical calculation.

5. Conclusion

We have proposed W-band photonic mm-wave vector signal generation based on a precoding-assisted random frequency tripling scheme, enabled by a single phase modulator cascaded with a WSS. The selected two optical subcarriers used to generate the frequency-tripling mm-wave vector signal have asymmetrical orders and can have several different kinds of combinations, such as (–3, 0), (–2, 1), (–1, 2), and (0, 3). Employing our proposed precoding-assisted random frequency tripling scheme, we have experimentally demonstrated the generation and 0.5-m wireless delivery of 1/2-Gbaud 81-GHz QPSK-modulated mm-wave vector signal. We have also experimentally demonstrated the generated mm-wave vector signal based on the –2nd and 1st subcarriers (equivalent to the –1st and 2nd subcarriers) has a better BER performance than that based on the –3rd and 0th subcarriers (equivalent to the 0th and 3rd subcarriers) when the phase modulator has a relatively small driving RF voltage, while an opposite result occurs when the phase modulator has a relatively large driving RF voltage, which is consistent with both our theoretical analysis and numerical simulation.

References

[1] X. Li, J. Xiao, and J. Yu, "Long-distance wireless mm-wave signal delivery at W-band," *J. Lightw. Technol.*, vol. 34, no. 2, pp. 661–668, Jan. 2016.

[2] X. Li, J. Yu, and J. Xiao, "Demonstration of ultra-capacity wireless signal delivery at W-band," *J. Lightw. Technol.*, vol. 34, no. 1, pp. 180–187, Jan. 2016.

[3] T. P. Mckenna, J. A. Nanzer, and T. R. Clark, "Experimental demonstration of photonic millimeter-wave system for high capacity point-to-point wireless communication," *J. Lightw. Technol.*, vol. 32, no. 20, pp. 3588–3594, Oct. 2014.

[4] K. Kitayama, A. Maruta, and Y. Yoshida, "Digital coherent technology for optical fiber and radio-over-fiber transmission systems," *J. Lightw. Technol.*, vol. 32, no. 20, pp. 3411–3420, Oct. 2014.

[5] J. Yu, X. Li, J. Zhang, and J. Xiao, "432-Gb/s PDM-16QAM signal wireless delivery at W-band using optical and antenna polarization multiplexing," presented at the Eur. Conf. Opt. Commun., Cannes, France, 2014, Paper We.3.6.6.

[6] X. Li, J. Yu, J. Xiao, and Y. Xu, "Fiber-wireless-fiber link for 128-Gb/s PDM-16QAM signal transmission at (*W*)-band," *IEEE Photon. Technol. Lett.*, vol. 26, no. 19, pp. 1948–1951, Oct. 2014.

[7] X. Li *et al.*, "Fiber-wireless-fiber link for 100-Gb/s PDM-QPSK signal transmission at W-band," *IEEE Photon. Technol. Lett.*, vol. 26, no. 18, pp. 1825–1828, Sep. 2014.

[8] J. Yu, X. Li, and N. Chi, "Faster than fiber: Over 100-Gb/s signal delivery in fiber wireless integration system," *Opt. Exp.*, vol. 21, no. 19, pp. 22885–22904, Sep. 2013.

[9] J. Zhang *et al.*, "Multichannel 120-Gb/s data transmission over 2 × 2 MIMO fiber-wireless link at W-band," *IEEE Photon. Technol. Lett.*, vol. 25, no. 8, pp. 780–783, Apr. 2013.

[10] X. Li *et al.*, "Fiber wireless transmission system of 108-Gb/s data over 80-km fiber and 2 × 2 MIMO wireless links at 100 GHz W-band frequency," *Opt. Lett.*, vol. 37, no. 24, pp. 5106–5108, Dec. 2012.

[11] F. Li, Z. Cao, X. Li, Z. Dong, and L. Chen, "Fiber-wireless transmission system of PDM-MIMO-OFDM at 100 GHz frequency," *J. Lightw. Technol.*, vol. 31, no. 14, pp. 2394–2399, Jul. 2013.

[12] A. Kanno *et al.*, "40 Gb/s W-band (75–110 GHz) 16-QAM radio-over-fiber signal generation and its wireless transmission," presented at the Eur. Conf. Exhib. Opt. Commun., Geneva, Switzerland, 2011, Paper We.10.P1.112.

[13] D. Zibar *et al.*, "High-capacity wireless signal generation and demodulation in 75- to 110-GHz band employing all optical OFDM," *IEEE Photon. Technol. Lett.*, vol. 23, no. 12, pp. 810–812, Jun. 2011.

[14] C. W. Chow *et al.*, "100 GHz ultra-wideband (UWB) fiber-to-the-antenna (FTTA) system for in-building and in-home networks," *Opt. Exp.*, vol. 18, no. 2, pp. 473–478, Jan. 2010.

[15] Y. Yang, C. Lim, and A. Nirmalathas, "Investigation on transport schemes for efficient high-frequency broadband OFDM transmission in fibre-wireless links," *J. Lightw. Technol.*, vol. 32, no. 2, pp. 267–274, Jan. 2014.

[16] J. Xiao, J. Yu, X. Li, Y. Xu, and Z. Zhang, "20-Gb/s PDM-QPSK signal delivery over 1.7-km wireless distance at W-band," presented at the Opt. Fiber Commun. Conf. Exhib., Los Angeles, CA, USA, 2015, Paper W4G.4.

[17] X. Li *et al.*, "Field trial of 80-Gb/s PDM-QPSK signal delivery over 300-m wireless distance with MIMO and antenna polarization multiplexing at W-band," presented at the Opt. Fiber Commun. Conf. Exhib., Los Angeles, CA, USA, 2015, Paper Th5A.5.

[18] X. Li, J. Yu, Z. Zhang, J. Xiao, and G. K. Chang, "Photonic vector signal generation at W-band employing an optical frequency octupling scheme enabled by a single MZM," *Opt. Commun.*, vol. 349, pp. 6–10, Aug. 2015.

[19] X. Li, J. Yu, J. Xiao, N. Chi, and Y. Xu, "W-band PDM-QPSK vector signal generation by MZM-based photonic frequency octupling and precoding," *IEEE Photon. J.*, vol. 7, no. 4, Aug. 2015, Art. no. 7101906.

[20] J. Xiao *et al.*, "W-band OFDM photonic vector signal generation employing a single Mach–Zehnder modulator and precoding," *Opt. Exp.*, vol. 23, no. 18, pp. 24029–24034, Sep. 2015.
[21] X. Li *et al.*, "Mm-wave vector signal generation and transport for W-band MIMO system with intensity modulation and direct detection," presented at the Opt. Fiber Commun. Conf. Exp., Anaheim, CA, USA, 2016, Paper M3B.2.
[22] X. Li *et al.*, "W-band QPSK vector signal generation based on photonic heterodyne beating and optical carrier suppression," presented at the Opt. Fiber Commun. Conf. Exp., Anaheim, CA, USA, 2016, Paper Th2A.15.
[23] X. Li *et al.*, "W-band 8QAM vector signal generation by MZM-based photonic frequency octupling," *IEEE Photon. Technol. Lett.*, vol. 27, no. 12, pp. 1257–1260, Jun. 2015.
[24] J. Xiao *et al.*, "High-frequency photonic vector signal generation employing a single phase modulator," *IEEE Photon. J.*, vol. 7, no. 2, Apr. 2015, Art. no. 7101206.
[25] C. T. Lin *et al.*, "Photonic vector signal generation at microwave/millimeter-wave bands employing an optical frequency quadrupling scheme," *Opt. Lett.*, vol. 34, no. 14, pp. 2171–2173, Jul. 2009.
[26] R. Zhang *et al.*, "Precoding research on vector signal 16QAM applied in the frequency doubling scheme of ROF link," presented at the Asia Commun. Photon. Conf., Beijing, China, 2013, Paper AF2F.2.
[27] X. Li *et al.*, "QAM vector signal generation by optical carrier suppression and precoding techniques," *IEEE Photon. Technol. Lett.*, vol. 27, no. 18, pp. 1977–1980, Sep. 2015.
[28] X. Li, J. Xiao, Y. Xu, and J. Yu, "QPSK vector signal generation based on photonic heterodyne beating and optical carrier suppression," *IEEE Photon. J.*, vol. 7, no. 5, Oct. 2015, Art. no. 7102606.
[29] J. Xiao *et al.*, "OFDM vector signal generation based on optical carrier suppression," *IEEE Photon. Technol. Lett.*, vol. 27, no. 23, pp. 2449–2452, Dec. 2015.
[30] Y. Wang, Y. Xu, X. Li, J. Yu, and N. Chi, "Balanced precoding technique for vector signal generation based on OCS," *IEEE Photon. Technol. Lett.*, vol. 27, no. 13, pp. 2469–2472, Dec. 2015.
[31] W. J. Jiang *et al.*, "Photonic vector signal generation employing a novel optical direct-detection in-phase/quadrature-phase upconversion," *Opt. Lett.*, vol. 35, no. 23, pp. 4069–4071, Dec. 2010.
[32] J. Yu *et al.*, "Optical millimeter-wave generation or up-conversion using external modulators," *IEEE Photon. Technol. Lett.*, vol. 18, no. 1, pp. 265–267, Jan. 2006.
[33] G. Qi, J. Yao, J. Seregelyi, S. Paquet, and C. Bélisle, "Optical generation and distribution of continuously tunable millimeter-wave signals using an optical phase modulator," *J. Lightw. Technol.*, vol. 23, no. 9, pp. 2687–2695, Sep. 2005.
[34] J. Yu, Z. Jia, T. Wang, and G. K. Chang, "A novel radio-over-fiber configuration using optical phase modulator to generate an optical mm-wave and centralized lightwave for uplink connection," *IEEE Photon. Technol. Lett.*, vol. 19, no. 3, pp. 140–142, Feb. 2007.
[35] H. C. Chien, Y. T. Hsueh, A. Chowdhury, and G. K. Chang, "A novel carrier-eliminated optical millimeter-wave generation using a single over-driven phase modulator," presented at the Conf. Opt. Fiber Commun., San Diego, CA, USA, 2010, Paper JWA55.
[36] J. Ma *et al.*, "Fiber dispersion influence on transmission of the optical millimeter-waves generated using LN-MZM intensity modulation," *J. Lightw. Technol.*, vol. 25, no. 11, pp. 3244–3256, Nov. 2007.
[37] J. Yu and X. Zhou, "Ultra-high-capacity DWDM transmission system for 100G and beyond," *IEEE Commun. Mag.*, vol. 48, no. 3, pp. S56–S64, Mar. 2010.